PROCEEDINGS, 50th Workshop on Geothermal Reservoir Engineering
Stanford University, Stanford, California, February 10-12, 2025
SGP-TR-229

Focal Mechanism and Stress Analysis of the CAPE Site, Utah

Ahmad Mohammadi[1], Xiaowei Chen[1], Nori Nakata[2], Sireesh Dadi[3]

[1]Department of Geology & Geophysics, Texas A&M University, 3115 TAMU, Berkeley, College Station, Texas 77843-3115

[2]Earth and Environmental Sciences Area, Lawrence Berkeley National Laboratory, 1 Cyclotron Rd., Berkeley, CA 94720

[3]Fervo Energy, Houston, TX 77002

a-mohamadi@tamu.edu

Keywords: Enhanced Geothermal Systems, seismic monitoring, microseismicity, Cape Modern

ABSTRACT

Microseismic monitoring plays a pivotal role in characterizing subsurface dynamics and assessing induced seismicity risks in Enhanced Geothermal Systems (EGS). This study presents a comprehensive analysis of microseismic data from the Cape Modern EGS field in Southwest Utah, where three horizontal wells underwent plug-and-perf hydraulic stimulation. The monitoring infrastructure comprised an integrated network of shallow borehole sensors, surface nodal arrays, deep borehole fiber optic sensors, and three-component passive sensors, capturing over 7,000 events during the February-March 2024 stimulation period. We implemented a multi-faceted analytical approach, beginning with phase arrival prediction and first motion polarity determination utilized deep learning techniques, while focal mechanism estimation employed the SKHASH method, incorporating P-wave polarity and S/P amplitude ratios. This methodology yielded 2,091 focal mechanism solutions, with 1,564 achieving high-quality (A and B) classifications. Subsequent clustering analysis using UMAP-HDBSCAN revealed four distinct structural features, with Structure D exhibiting complex spatial patterns and multiple sub-clusters. Stress field analysis using MSATSI demonstrated significant spatial heterogeneity, transitioning from strike-slip dominated regimes in the western section (SHmax 15-30° from North) to reverse faulting patterns in the eastern section (SHmax 0-15° from North). The stress ratio variations indicate complex mechanical interactions between stimulation operations and local geological structures. These findings provide crucial insights for optimizing EGS operations while highlighting the effectiveness of integrating machine learning techniques with traditional geophysical methodologies for enhanced reservoir characterization.

INTRODUCTION

Geothermal energy exploitation has evolved significantly since its initial development at Larderello, Italy in 1904, where the first electricity-generating geothermal power plant was constructed (Burgassi 1999). The concept of Enhanced Geothermal Systems (EGS) emerged in the 1970s at Fenton Hill, New Mexico, introducing methodologies for creating artificial reservoirs in hot dry rock (HDR) formations through hydraulic stimulation (Brown et al. 2012). These systems typically operate by inducing controlled hydraulic fracturing at depths ranging from 3-10 km, where temperatures exceed 150°C, to establish sufficient permeability for sustainable heat extraction (Tester et al. 2006). Microseismic monitoring has become an indispensable tool for EGS development, enabling real-time characterization of fracture network evolution and reservoir dynamics through analysis of induced seismicity patterns and moment tensor solutions (Majer et al. 2007).

Microseismic activity in Enhanced Geothermal Systems (EGS) arises from the injection of high-pressure fluids into subsurface formations, a process designed to improve rock permeability by stimulating pre-existing fractures or creating new ones. Since the 1970s, when hydraulic fracturing was first applied to geothermal reservoirs such as the Fenton Hill project in New Mexico, microseismic monitoring has played a pivotal role in understanding reservoir dynamics (Brown et al. 2012). Early techniques relied on sparse networks of geophones to detect seismic events and infer fracture propagation. However, as EGS projects expanded globally, dense seismic arrays became essential to capture the complex spatial and temporal patterns of induced seismicity (Majer et al. 2007).

Over time, advancements in data analysis techniques have further refined the interpretation of microseismic data. The development of moment tensor inversion methods provided insights into the mechanisms of induced events, distinguishing between shear and tensile failure modes. Modern seismic monitoring now incorporates cutting-edge machine learning (ML) and deep learning (DL) approaches to enhance the detection, classification, and analysis of microseismicity. For instance, convolutional neural networks (CNNs) have been employed to automate the detection and phase picking of seismic events, dramatically reducing manual processing time (Perol, Gharbi, and Denolle 2018). Similarly, recurrent neural networks (RNNs) and long short-term memory (LSTM) models are being used to predict future seismic events based on temporal patterns in microseismic data (Mousavi et al. 2020). The integration of ML and DL techniques into microseismic monitoring has not only enhanced the resolution and accuracy of subsurface imaging but has also provided new ways to understand the underlying geomechanics of EGS reservoirs. By combining traditional geophysical methods with these computational advances, researchers can more effectively optimize fluid injection strategies, mitigate seismic risks, and improve the overall sustainability of geothermal energy production.

Focal mechanism and stress inversion techniques have been essential in understanding the stress state and faulting behavior in EGS reservoirs. Focal mechanism solutions, which describe the orientation of fault planes and slip directions, have historically been derived from the polarity of first P-wave arrivals (Reasenberg and Oppenheimer 1986; Hardebeck and Shearer 2002). The advent of moment

tensor inversion allowed for more accurate and comprehensive characterization of seismic sources, providing insights into the types of faulting and the presence of tensile or shear failure (Hardebeck and Shearer 2002; 2003). Stress inversion techniques, which infer the regional stress field from multiple focal mechanism solutions, have been instrumental in identifying the principal stress directions and understanding how stress perturbations from fluid injections influence fault reactivation. For example, stress inversion studies at the Geysers geothermal field in California have revealed a highly heterogeneous stress field, reflecting the complex interactions between natural tectonic stresses and those induced by reservoir operations (Martínez-Garzón et al. 2013).

The Cape Modern project, a next generation Enhanced Geothermal System (EGS) field, is being developed in Southwest Utah (Nakata et al., 2024). The initial phase of the project involved stimulating three horizontal wells using the plug-and-perf hydraulic stimulation technique. To monitor induced seismicity effectively, an advanced microseismic network was deployed, including shallow borehole sensors, a surface nodal array, deep borehole fiber optic sensors, and 3-component (3C) passive sensors. This paper presents findings from microseismic monitoring using data from shallow borehole arrays, deep borehole fiber optics, and 3C geophones.

2. DATA

The field infrastructure comprises five deep wells: one vertical monitoring well (Delano 1-OB) and four horizontal wells (Frisco 1-I, 2-P, 3-I, and 4-T). The horizontal wells are configured as two injector-producer pairs, with Frisco 1-I and 3-I serving as injection wells and Frisco 2-P and 4-T functioning as production wells (Figure 1). The injection wells are positioned at greater depths relative to the production wells. The vertical monitoring well, Delano 1-OB, extends beyond the depth of both injector and producer wells and is instrumented with permanent fiber optic monitoring capabilities behind the casing to facilitate microseismic monitoring at depths exceeding those of the horizontal well network.

The stimulation program was executed in two distinct phases, with this study focusing on the initial phase conducted in February/March 2024. During this period, stimulation operations were completed on all stages of Frisco 1-I and 3-I wells, along with two stages of Frisco 2-P. Seismic monitoring during stimulation operations was accomplished through a comprehensive network consisting of 258 three-component geophones deployed in a surface nodal array by Lawrence Berkeley National Laboratory (LBNL), recording continuous waveform data at a sampling rate of 1000 Hz. This network was supplemented by seven shallow borehole stations.

Microseismic event detection and location were performed by Fervo Energy using distributed acoustic sensing (DAS) data from the deep borehole fiber optic installation, combined with three-component sensor data from well 56-32. Event selection criteria prioritized high signal-to-noise ratio (SNR) recordings from the LBNL nodal array, resulting in a refined catalog of 2,211 events. For each identified event, waveform data were extracted spanning a window from one second before to nine seconds after the determined origin time.

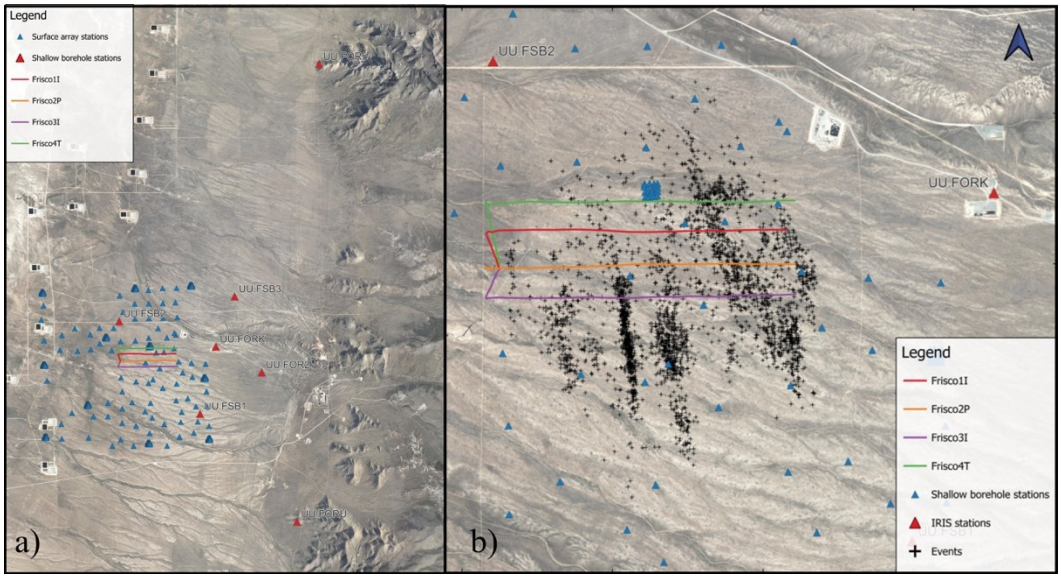

Figure 1: Map View of the temporary monitoring (blue triangle) and the permanent shallow borehole (red triangle) stations. The four stimulation wells are shown by colored solid lines, and the microseismic events are shown by black "+". (a) shows an overall map view of the recording system, and (b) shows zoom-in view of the stimulation system.

3. METHODS AND RESULTS

3.1 Focal Mechanism Estimation

The advanced phase-picking methodologies leverage artificial intelligence (AI) and demonstrate statistically significant improvements over conventional algorithmic approaches, achieving phase-timing precision comparable to expert analysts while exhibiting superior temporal efficiency. The enhanced capabilities of these systems are particularly evident in traditionally challenging seismological scenarios: S-wave arrival determination in complex wave trains and phase identification in low signal-to-noise ratio (SNR) environments

(Mousavi and Beroza 2023). We used the EQNet (a new version of PhasNet) model to predict the P and S arrival times and phase polarity for the events in our catalog (Zhu and Beroza 2019). P-wave polarity was determined from the EQNet phase polarity values observed on the vertical component. For relative amplitude determination, all waveforms underwent bandpass filtering between 1-55 Hz and were subsequently rotated to their radial and tangential components. P-wave amplitude was calculated as the Cartesian summation of the P-phase on the radial and vertical components, while S-wave amplitude was determined by selecting the maximum amplitude among the radial, tangential, and vertical components during the S-phase arrival window. To ensure data quality for focal mechanism estimation, after the phase prediction step, we only selected picks that the P phase score has a value of 0.8 or greater for the rest of our focal mechanism estimation.

For focal mechanism determination, we utilized SKHASH, a Python implementation and modernization of the established HASH package originally developed in Fortran two decades ago (Hardebeck and Shearer 2002; Skoumal, Hardebeck, and Shearer 2024). SKHASH incorporates recent methodological advances to better constrain focal mechanisms for small magnitude and sparsely recorded earthquakes. The algorithm evaluates multiple acceptable solutions by systematically varying earthquake locations and velocity models. Our implementation incorporated both P-wave first motion polarity and S/P amplitude ratios as input constraints. To minimize location-dependent uncertainties, we explicitly accounted for both horizontal and vertical location uncertainties in the inversion process.

The analysis resulted in 2,091 focal mechanism solutions, of which 1,564 were rated as high quality (A and B) according to the SKHASH uncertainty criteria. To classify the faulting regimes, we employed the classification scheme of Zoback (1992), which categorizes seismic events into three primary types: strike-slip (SS), normal faulting (NF), and thrust faulting (TF). Additionally, hybrid faulting categories were identified, including trans-tension (NS, a combination of normal and strike-slip) and trans-pression (TS, a combination of thrust and strike-slip). However, further analysis using the Kaverina (1996) source mechanism diagram of focal mechanism indicated that many of these "Unknown" events exhibited characteristics leaning toward thrust faulting behavior (Figure 2). The classification results revealed that most of the events were strike-slip, with 766 classified as SS. Other categories included 296 TF events, 40 NF events, 14 NS events, and 11 TS events. Notably, 437 events remained classified as "Unknown".

The spatial distribution of focal mechanisms highlighted distinct structural domains across the study area. The western sector predominantly featured strike-slip mechanisms, reflecting relatively simple structural patterns. Conversely, the eastern and northeastern sectors were marked by greater structural complexity, characterized by a mix of reverse and strike-slip faulting patterns (Figure 3). In the western region, the faulting behavior remained consistent from deeper to shallower depths, aligning with the simpler structural framework. In contrast, the eastern and northeastern regions, located closer to the injection point, exhibited significant variation in faulting patterns with depth, reflecting the more intricate structural dynamics in these areas.

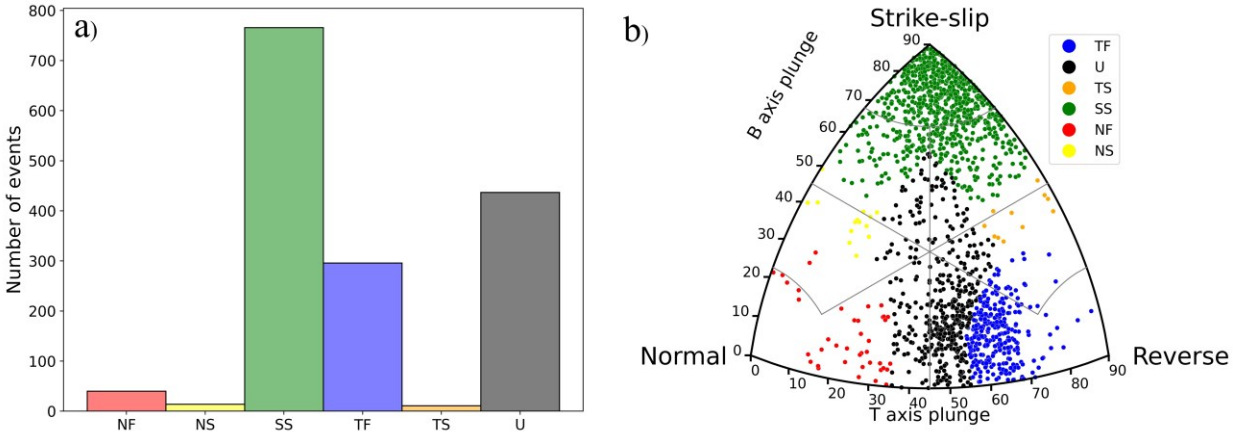

Figure 2: Faulting regime distribution using Zoback (1992) (a) and focal mechanisms diagram using Kaverina (1996) (b). The color code on the focal mechanisms diagram follows the color code of the faulting regime distribution. SS: Strike-Slip, NF: Normal Faulting, TF: Thrust Faulting, NS: Trans-Tension, TS: Trans-Pression U: Unknown.

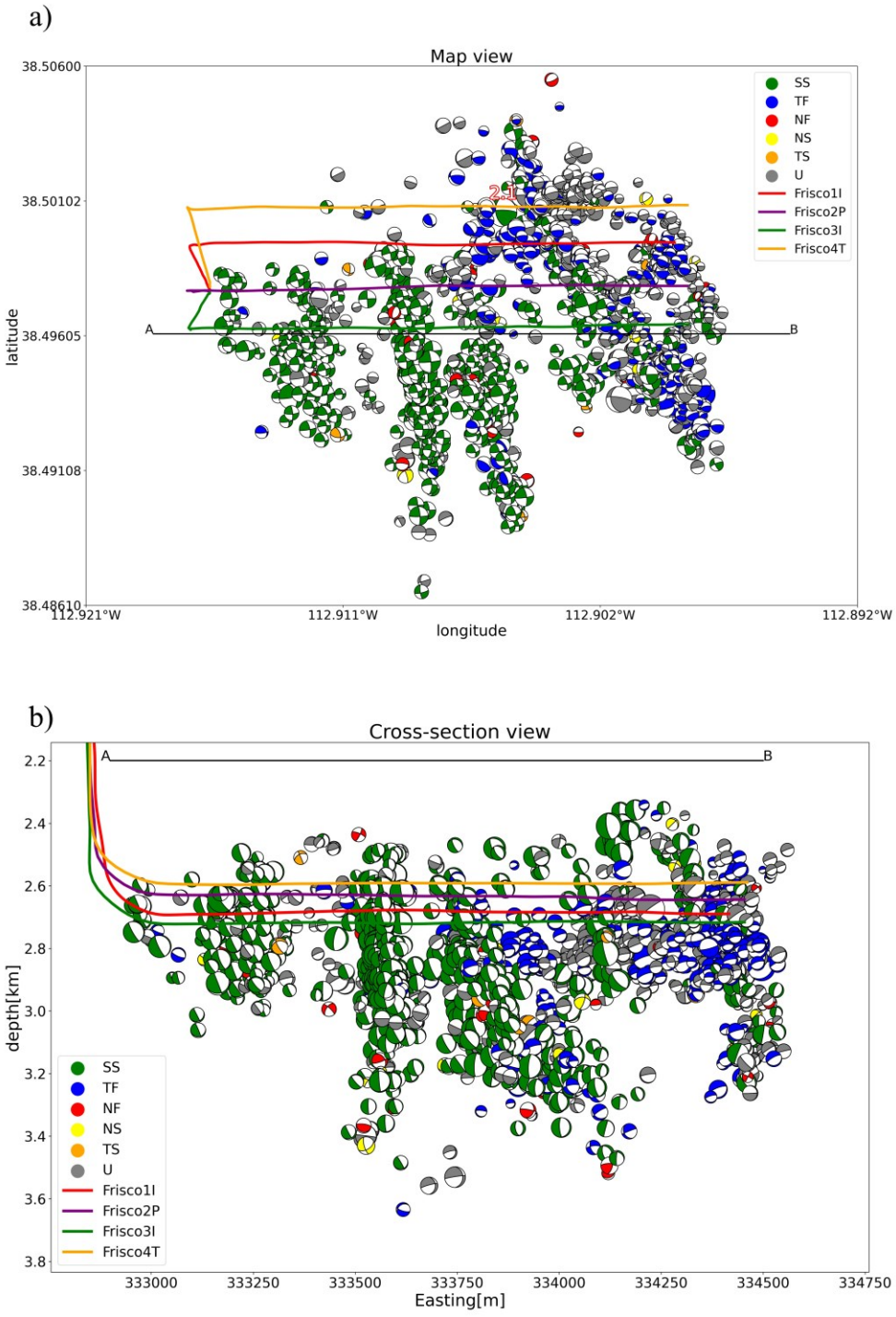

Figure 3: Map view (a) and cross-section view (b) of the high-quality (A and B quality) focal mechanism solutions, colored coded by the faulting regime.

3.2 Clustering

To systematically characterize fracture patterns within the study area, we implemented an advanced machine learning-based clustering framework. Although the seismic events exhibited spatial confinement, the region's inherent structural heterogeneities necessitated sophisticated analytical approaches. We employed the Uniform Manifold Approximation and Projection (UMAP) algorithm, a state-of-the-art non-linear dimensionality reduction technique (McInnes et al. 2020). UMAP's capacity to preserve global topological structure

while maintaining computational efficiency makes it particularly advantageous for complex seismological datasets where the preservation of structural relationships is critical.

The time evolution of events initiation shows that in some parts of the study area, although the distance between events is close but there is a gap in time activation of the events (Figure 4). To incorporate time as an input for our clustering at the initial analysis phase we involved UMAP-based dimensionality reduction from a four-dimensional feature space comprising spatial coordinates (x, y, z) and time to a three-dimensional manifold. Hyperparameter optimization yielded 50 nearest neighbors, and a minimum distance configured to identify high-density cluster formations. The resulting three-dimensional UMAP embedding underwent subsequent analysis using Hierarchical Density-Based Spatial Clustering (HDBSCAN) (Campello et al. 2013). The HDBSCAN implementation utilized a minimum cluster size of 50 and a minimum sample threshold of 15 to establish preliminary cluster boundaries. To enhance cluster resolution and mitigate noise effects, we performed a secondary density-based clustering iteration with identical hyperparameters, constrained to three spatial components per cluster, facilitating sub-cluster identification. The final clustering solution incorporated strict quality controls, excluding sub-clusters with fewer than 30 events and restricting analysis to events with high-quality focal mechanisms (qualities A and B).

The clustering analysis revealed four distinct structural features (A, B, C, and D) that demonstrated activity during the stimulation period (Figure 5). Clusters number a1 and b1 belong to the structures A and B respectively and Structure C consists of two clusters c1 and c2. Structure D exhibited the highest structural complexity, encompassing four distinct clusters and displaying vertical extension from deeper to shallower reservoir sections, with a distinctive South-East to North-West orientation that deviated from other identified structures. Clusters d1, d2, and d3, spatially correlated with injection well depths, demonstrated predominant reverse faulting mechanisms. Conversely, cluster d4, situated in the deeper structural domain, exhibited characteristic strike-slip faulting patterns. Notable seismic events of maximum magnitude were spatially associated with the deeper structural sections. Temporal analysis of event initiation sequences (Figure 4) revealed a progressive activation pattern, initiating with Clusters d2 and d3, followed by Cluster b1, and culminating in the activation of Clusters d1 and d4.

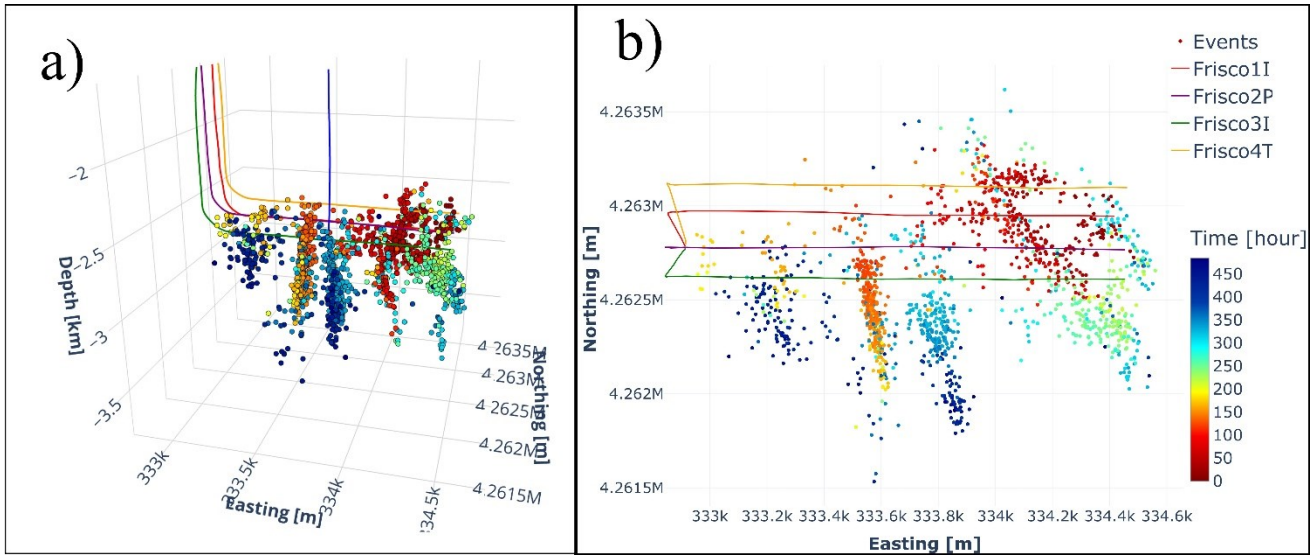

Figure 4: (a) 3D and (b) top view of the events to show time evaluation of the events activation. The color bar shows the time in hour based on the origin time of the first event activated in the catalog.

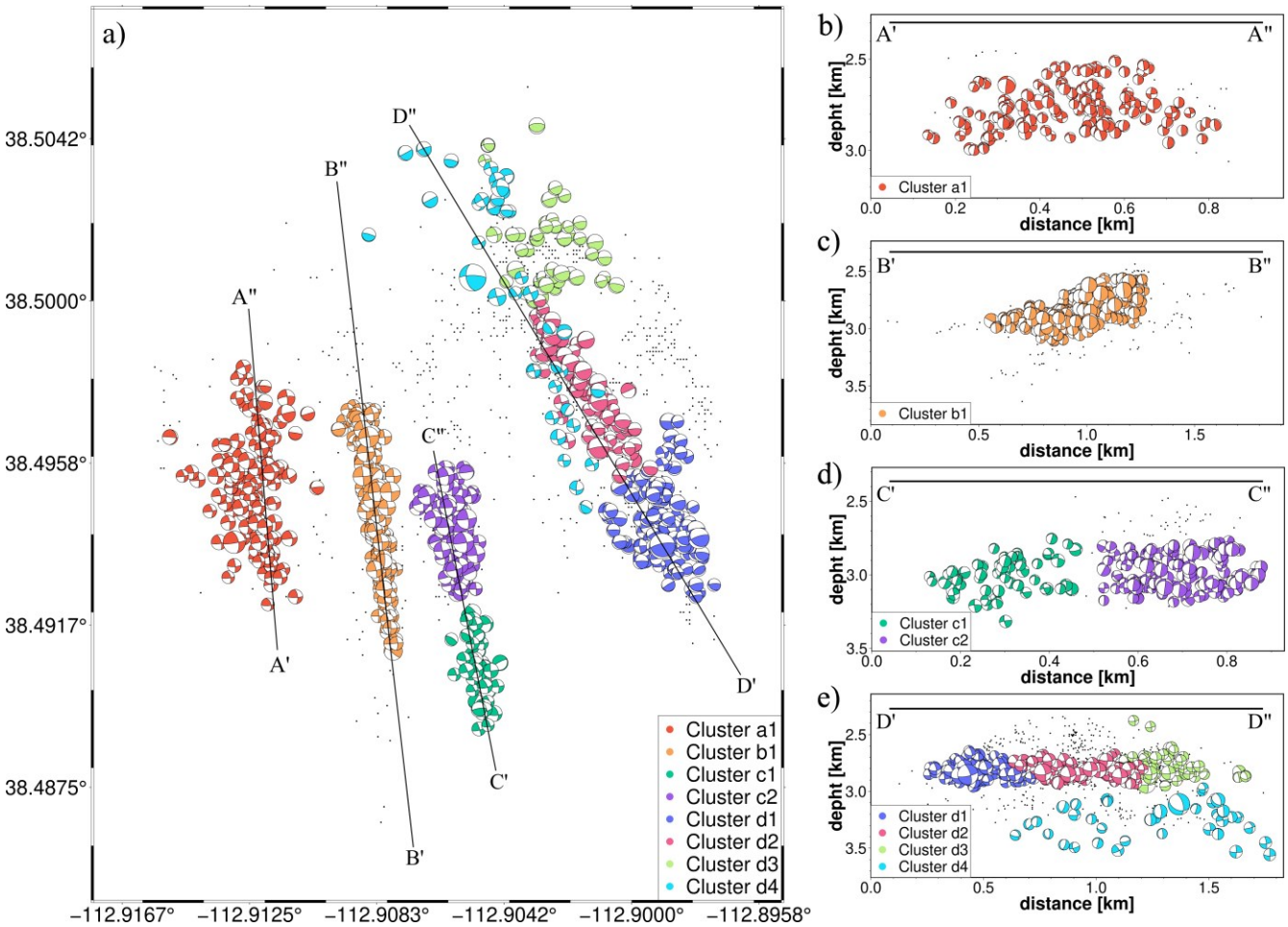

Figure 5: Top view and cross-sectional view of the clustering result. Beachballs are color-coded based on the clusters and grey dots show non-clustered events. (a) shows the top view of all clusters and on the right-hand side the cross-sectional view (b), (c), (d), and (e) are related to each structures A, B, C, and D respectively.

3.3 Stress Inversion

To get a better understanding of the study area we performed stress inversion by using the MSATSI software package (Martínez-Garzón et al. 2014). MSATSI is a MATLAB implementation that builds upon the methodological framework of SATSI (Hardebeck and Michael 2006), which itself represents a modified version of Michael 1984) foundational algorithms for inverting stress fields from earthquake focal mechanism solutions. The software operates under several fundamental assumptions about the nature of seismic events and stress fields. First, it assumes that tectonic stress maintains uniformity throughout the analyzed region. Second, it posits that seismic events occur primarily along pre-existing fault structures with diverse orientations rather than through the formation of new faults. Third, it incorporates the Wallace–Bott hypothesis (Bott 1959; Wallace 1951), which states that the slip vector aligns with the direction of shear stress acting on the fault plane. Through this mathematical framework, MSATSI performs inversions that yield two primary outputs characterizing the stress field: the three-dimensional orientations of the principal stress axes (σ1, σ2, and σ3), and a scalar parameter R=(σ1- σ2)/(σ1- σ3) that quantifies the relative magnitudes of these principal stresses. This stress ratio R provides crucial information about the relationship between the intermediate principal stress (σ2) relative to the maximum (σ1) and minimum (σ3) principal stresses, offering insights into the nature of the stress regime in the studied region.

We conducted stress tensor inversions on the previously identified seismic clusters to elucidate the spatial variations in the stress field. The inversion methodology incorporated both nodal plane solutions as input parameters to comprehensively assess possible fault orientations. To mitigate the influence of uncertainty in focal mechanism determinations, we used 1000 bootstrap resampling iterations during the inversion process. The spatial distribution of stress tensors reveals systematic variations across the study region (Figure 6). A notable transition in faulting style is observed, characterized by a progression from strike-slip to reverse faulting mechanisms as proximity to the injection point increases. This pattern is particularly evident in clusters d1, d2, and d3, which are spatially proximal to the injection point and exhibit predominantly reverse faulting behavior. In contrast, cluster d4, situated at greater depths, demonstrates a strike-slip regime with an elevated stress ratio (R) value, indicating minimal differential stress between the intermediate (σ2) and minimum (σ3)

principal stress axes. Also, clusters with reverse stressing regime have their Shmax orientated toward 0-15 degrees from North but the clusters with strike-slip stressing regime have Shmax orientated toward 15-30 degrees from North.

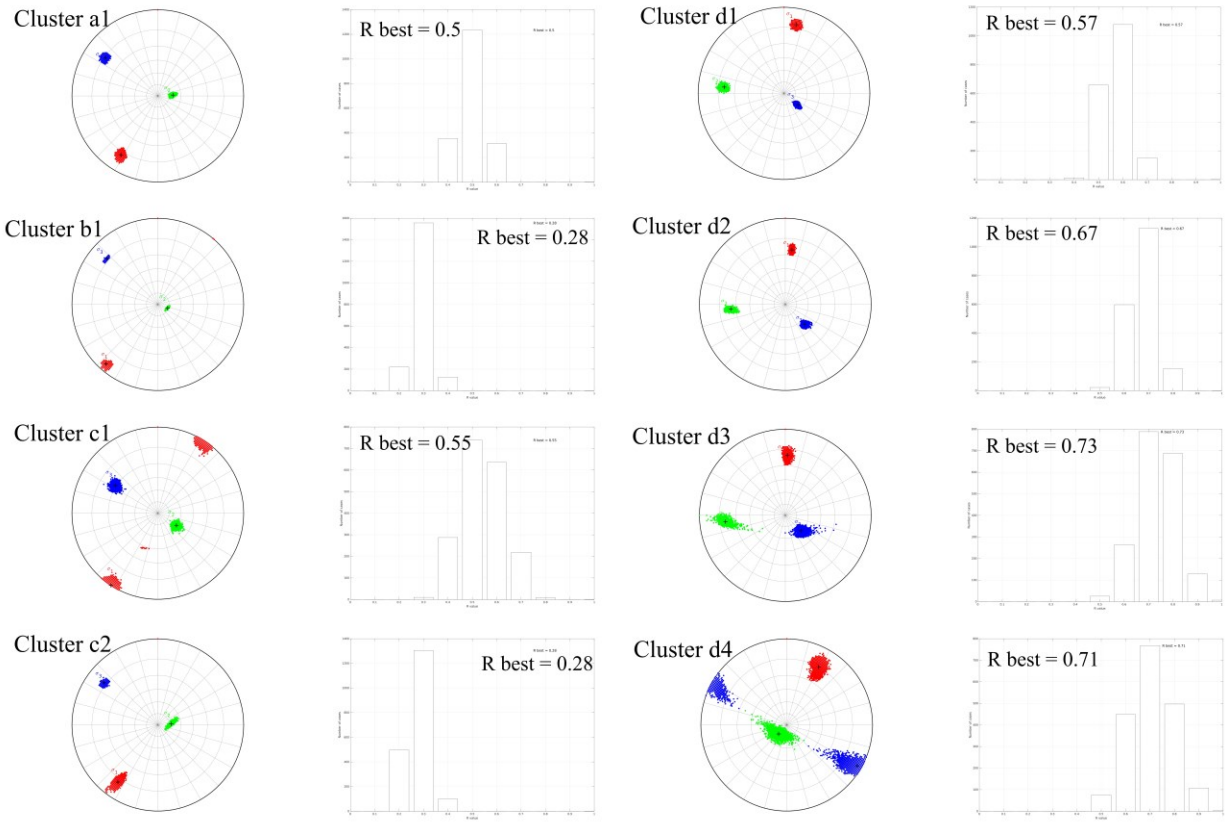

Figure 6: MSATSI output result of the stress inversion for each cluster. The azimuth and plunge of the three principal components σ1 (red), σ2 (green), and σ3(blue) are shown on the stereonet plot for each cluster alongside the histogram of the stress ratio value R.

6. CONCLUSION

Comprehensive analysis of microseismic data from the Cape Modern Geothermal System has revealed significant insights into the complex subsurface dynamics associated with hydraulic stimulation operations. Through the integration of advanced machine learning techniques and traditional geophysical methodologies, we successfully characterized over 2,000 seismic events, yielding 1,564 high-quality focal mechanisms that illuminate the structural complexity of the reservoir system.

The spatial distribution of focal mechanisms demonstrates distinct structural domains across the study area, with a clear transition from predominantly strike-slip mechanisms in the western sector to a more complex mixture of reverse and strike-slip faulting patterns in the eastern and northeastern sectors. This spatial heterogeneity reflects the underlying structural framework and its response to stimulation operations. The implementation of the UMAP-HDBSCAN clustering framework identified four primary structural features (A-D), with Structure D exhibiting particularly complex behavior characterized by multiple sub-clusters and distinctive spatial orientation.

Stress tensor inversions reveal systematic variations in the stress field across the study area, with a notable transition in faulting style proximal to injection points. The observed progression from strike-slip to reverse faulting mechanisms near injection zones, coupled with variations in SHmax orientation (0-15 degrees from North in reverse stress regimes versus 15-30 degrees in strike-slip regimes), suggests significant stress perturbations induced by stimulation operations. The elevated stress ratio (R) values in deeper clusters, particularly cluster 5, indicate minimal differential stress between σ_2 and σ_3 principal stress axes, providing crucial insights into the mechanical behavior of the reservoir system.

These findings have significant implications for optimizing future EGS operations at the Cape Modern site and similar geological settings. The observed spatial variations in stress patterns and structural responses to stimulation highlight the importance of adaptive injection strategies that account for local structural complexity. Furthermore, the successful application of machine learning techniques in phase picking and event classification demonstrates the value of integrating advanced computational methods with traditional geophysical approaches for enhanced reservoir characterization and monitoring.

Future research directions should focus on investigating the temporal evolution of stress perturbations during extended operation periods and estimating the non-double component of the moment tensor. Additionally, the integration of real-time monitoring systems with machine learning-based analysis could enable more responsive and efficient reservoir management strategies while maintaining operational safety and sustainability.

REFERENCES

Bott, M. H. P. 1959. "The Mechanics of Oblique Slip Faulting." *Geological Magazine* 96 (2): 109–17. https://doi.org/10.1017/S0016756800059987.

Brown, Donald W, David V Duchane, Grant Heiken, and Vivi Thomas Hriscu. 2012. *Mining the Earth's Heat: Hot Dry Rock Geothermal Energy*. Springer Science & Business Media.

Burgassi, Pier Domenico. 1999. "Historical Outline of Geothermal Technology in the Larderello Region to the Middle of the 20th Century." *Stories from a Heated Earth*, 195–219.

Campello, Ricardo J. G. B., Davoud Moulavi, and Joerg Sander. 2013. "Density-Based Clustering Based on Hierarchical Density Estimates." In *Advances in Knowledge Discovery and Data Mining*, edited by Jian Pei, Vincent S. Tseng, Longbing Cao, Hiroshi Motoda, and Guandong Xu, 160–72. Berlin, Heidelberg: Springer. https://doi.org/10.1007/978-3-642-37456-2_14.

Hardebeck, Jeanne L, and Andrew J Michael. 2006. "Damped Regional-Scale Stress Inversions: Methodology and Examples for Southern California and the Coalinga Aftershock Sequence." *Journal of Geophysical Research: Solid Earth* 111 (B11).

Hardebeck, Jeanne L, and Peter M Shearer. 2002. "A New Method for Determining First-Motion Focal Mechanisms." *Bulletin of the Seismological Society of America* 92 (6): 2264–76.

Hardebeck, Jeanne L., and Peter M. Shearer. 2003. "Using S/P Amplitude Ratios to Constrain the Focal Mechanisms of Small Earthquakes." *Bulletin of the Seismological Society of America* 93 (6): 2434–44. https://doi.org/10.1785/0120020236.

Kaverina, A. N., A. V. Lander, and A. G. Prozorov. 1996. "Global Creepex Distribution and Its Relation to Earthquake-Source Geometry and Tectonic Origin." *Geophysical Journal International* 125 (1): 249–65. https://doi.org/10.1111/j.1365-246X.1996.tb06549.x.

Majer, Ernest L, Roy Baria, Mitch Stark, Stephen Oates, Julian Bommer, Bill Smith, and Hiroshi Asanuma. 2007. "Induced Seismicity Associated with Enhanced Geothermal Systems." *Geothermics* 36 (3): 185–222.

Martínez-Garzón, Patricia, Marco Bohnhoff, Grzegorz Kwiatek, and Georg Dresen. 2013. "Stress Tensor Changes Related to Fluid Injection at The Geysers Geothermal Field, California." *Geophysical Research Letters* 40 (11): 2596–2601. https://doi.org/10.1002/grl.50438.

Martínez-Garzón, Patricia, Grzegorz Kwiatek, Michèle Ickrath, and Marco Bohnhoff. 2014. "MSATSI: A MATLAB Package for Stress Inversion Combining Solid Classic Methodology, a New Simplified User-Handling, and a Visualization Tool." *Seismological Research Letters* 85 (4): 896–904. https://doi.org/10.1785/0220130189.

McInnes, Leland, John Healy, and James Melville. 2020. "UMAP: Uniform Manifold Approximation and Projection for Dimension Reduction." arXiv. https://doi.org/10.48550/arXiv.1802.03426.

Michael, Andrew J. 1984. "Determination of Stress from Slip Data: Faults and Folds." *Journal of Geophysical Research: Solid Earth* 89 (B13): 11517–26. https://doi.org/10.1029/JB089iB13p11517.

Mousavi, S Mostafa, and Gregory C Beroza. 2023. "Machine Learning in Earthquake Seismology." *Annual Review of Earth and Planetary Sciences* 51 (1): 105–29.

Mousavi, S Mostafa, William L Ellsworth, Weiqiang Zhu, Lindsay Y Chuang, and Gregory C Beroza. 2020. "Earthquake Transformer—an Attentive Deep-Learning Model for Simultaneous Earthquake Detection and Phase Picking." *Nature Communications* 11 (1): 3952.

Nakata, Nori, Sin-Mei Wu, Chet Hopp, Michelle Robertson, and Sireesh Dadi. n.d. "Microseismicity Observation and Characterization at Cape Modern and Utah FORGE."

Perol, Thibaut, Michaël Gharbi, and Marine Denolle. 2018. "Convolutional Neural Network for Earthquake Detection and Location." *Science Advances* 4 (2): e1700578. https://doi.org/10.1126/sciadv.1700578.

Reasenberg, Paul, and David Oppenheimer. 1986. *FPFIT, FPPLOT and FPPAGE: Fortran Computer Programs for Calculating and Displaying Earthquake Fault-Plane Solutions*. Vol. 85. 739. US Geological Survey.

Skoumal, Robert J., Jeanne L. Hardebeck, and Peter M. Shearer. 2024. "SKHASH: A Python Package for Computing Earthquake Focal Mechanisms." *Seismological Research Letters* 95 (4): 2519–26. https://doi.org/10.1785/0220230329.

Tester, Jefferson W, Brian J Anderson, Anthony S Batchelor, David D Blackwell, Ronald DiPippo, Elisabeth M Drake, John Garnish, et al. 2006. "The Future of Geothermal Energy." *Massachusetts Institute of Technology* 358:1–3.

Wallace, Robert E. 1951. "Geometry of Shearing Stress and Relation to Faulting." *The Journal of Geology* 59 (2): 118–30. https://doi.org/10.1086/625831.

Zhu, Weiqiang, and Gregory C Beroza. 2019. "PhaseNet: A Deep-Neural-Network-Based Seismic Arrival-Time Picking Method." *Geophysical Journal International* 216 (1): 261–73.

Zoback, Mary Lou. 1992. "First-and Second-Order Patterns of Stress in the Lithosphere: The World Stress Map Project." *Journal of Geophysical Research: Solid Earth* 97 (B8): 11703–28.